

UDC 666.3

DYSPROSIUM-DOPING INFLUENCE ON THE MICROSTRUCTURE AND TEXTURING OF BISMUTH-TELLURIDE THERMOELECTRIC MATERIALS

M. N. Yaprincev¹ and O. N. Ivanov²

Translated from *Steklo i Keramika*, No. 8, pp. 39–47, August, 2023.

Original article submitted April 28, 2023.

The preparation and identification of microstructure features as well as the texturing of the thermoelectric material $\text{Bi}_2\text{Te}_{2.7}\text{Se}_{0.3}$ doped with dysprosium are considered. The textured compounds $\text{Bi}_{2-x}\text{Dy}_x\text{Te}_{2.7}\text{Se}_{0.3}$ with $x = 0.0000; 0.0010; 0.0025; 0.0050; 0.0100$, and 0.0200 were obtained by means of solvothermal synthesis of the original powders and their subsequent spark plasma sintering. Dysprosium doping effects several interrelated phenomena. The first one is particle size reduction of the original powder with increasing x . This effect is explained by an increase in the ionicity of the covalently polar bonds $\text{Bi}(\text{Dy})\text{-Te}$ with increasing Dy content on account of the difference in the electro-negativity of Bi and Dy. The second effect is associated with average grain size reduction with increasing x in bulk samples, which is determined by a corresponding change in the particle size in the original powder with different amounts of alloying. This phenomenon also effects greater texturing in the samples.

Keywords: thermoelectric materials, crystallographic texture, rare-earth doping, microstructure, spark plasma sintering.

INTRODUCTION

Although significant progress has been made in the last decade in increasing the thermoelectric quality-factor (ZT) of thermoelectric materials, the commercial use of thermoelectric devices is still significantly limited by their low energy efficiency [1]. The maximum thermoelectric quality-factor of materials used in industry does not exceed 1 ($ZT \leq 1$), which greatly restricts their widespread use and stimulates the search and development of new scientific and technical approaches to their modification in order to increase the thermoelectric quality-factor. The thermoelectric properties of materials can be optimized in different ways (alloying, creation of solid solutions, nanostructuring, etc.). A promising scientific approach to increasing ZT is based on the formation of a specific defect structure in doped semiconductors, effecting resonant impurity energy levels in the conduction or valence band. This approach can be implemented by lanthanide doping of thermoelectric materials. It

is also important that the interaction of localized magnetic moments of 4- f elements with the spin of conduction electrons can substantially increase in the Seebeck coefficient [2, 3].

The *intent of present work* is to obtain the thermoelectric materials $\text{Bi}_{2-x}\text{Dy}_x\text{Te}_{2.7}\text{Se}_{0.3}$ ($x = 0.0000, 0.0010, 0.0025, 0.0050, 0.0100$, and 0.0200) and to ascertain the predictables of the influence of doping on the microstructural aspects of the materials.

The preparation of these materials is of interest for several reasons. Firstly, dysprosium has a large number of unpaired electrons in the 4- f electronic level, so that on doping telluride-based compounds with dysprosium, can effect formation of resonant levels [4]. Secondly, dysprosium has the largest intrinsic magnetic moment among the lanthanides, which can result in higher Seebeck coefficients on account of the appearance of different spin effects [5]. In addition, the non-doped compound $\text{Bi}_2\text{Te}_{2.7}\text{Se}_{0.3}$ has the highest thermoelectric quality-factor among materials based on bismuth telluride with electronic conductivity and finds widespread commercial applications. For this reason, the preparation of doped compounds in which doping is aimed at increasing their thermoelectric quality-factor is of great practical importance.

¹ Belgorod State National Research University, Belgorod, Russia (e-mail: yaprincev@bsu.edu.ru).

² V. G. Shukhov Belgorod State Technological University, Belgorod, Russia (e-mail: olniv@mail.ru).

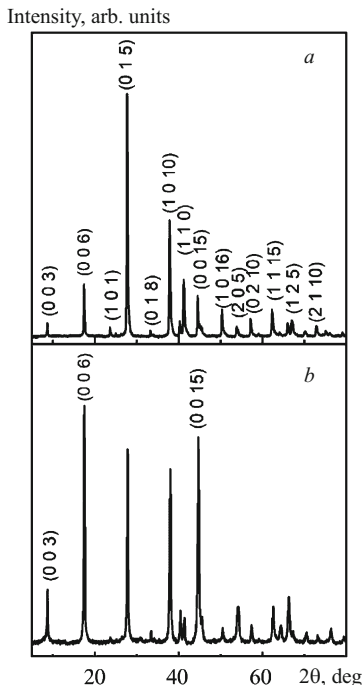


Fig. 1. Diffraction patterns of the initial powder of the compound $\text{Bi}_{1.98}\text{Dy}_{0.02}\text{Te}_{2.7}\text{Se}_{0.3}$ (a) and the bulk polycrystalline material based on it (b); the diffraction pattern was obtained from the surface perpendicular to the direction of application of pressure during the sintering process.

In this work, the microstructure of the polycrystalline compounds $\text{Bi}_{2-x}\text{Dy}_x\text{Te}_{2.7}\text{Se}_{0.3}$ is characterized by the average grain size and the degree of grain ordering. Both of these microstructural parameters have a noticeable effect on the thermoelectric properties of polycrystalline compounds based on bismuth telluride: grain boundaries are scattering centers for electrons and phonons, which largely determines the electrical conductivity and thermal conductivity of the material, respectively, and grain ordering effects partial restoration of the anisotropy of the thermoelectric properties of polycrystalline materials, characteristic of single crystals, and the possibility of choosing the optimal orientation of samples with the maximum thermoelectric quality-factor.

SAMPLE PREPARATION AND INVESTIGATIVE PROCEDURES

The compound $\text{Bi}_{2-x}\text{Dy}_x\text{Te}_{2.7}\text{Se}_{0.3}$ was prepared by means of solvothermal synthesis of the initial powders and followed by spark plasma sintering. The starting powders were synthesized using analytically pure grade chemical substances ($\text{Bi}(\text{NO}_3)_3 \cdot 5\text{H}_2\text{O}$, TeO_2 , SeO_2 , $\text{Dy}(\text{NO}_3)_3 \cdot 6\text{H}_2\text{O}$, NaOH, ethane-1,2-diol). At the first stage of synthesis, $\text{Bi}(\text{NO}_3)_3 \cdot 5\text{H}_2\text{O}$, TeO_2 , and $\text{Dy}(\text{NO}_3)_3 \cdot 6\text{H}_2\text{O}$, taken in stoichiometric ratio with dysprosium taken into account per 30 g of product were dissolved in a mixture of 1000 cm^3 of ethane-1,2-diol and 20 g of NaOH with intense mixing by a

magnetic mixer. After full dissolution, the volume of the reaction medium was adjusted to 1500 cm^3 by adding ethane-1,2-diol and then heated to boiling temperature. On intense boiling the system was kept open for 15 min to remove water, after which the system was equipped with a reflux condenser and a water seal to prevent contact with air. Isothermal soaking was conducted at 185°C for 6 h, after which the system was allowed to cool down to room temperature naturally. At the completion of the reaction a dark gray precipitate was separated by centrifuging, washed several times with isopropyl alcohol, and dried at 80°C for 8 h. Compaction was conducted using a model 10-3 spark plasma sintering system (Thermal Technology, LLC, USA). The sintering parameters were: pressure 40 MPa, temperature 680 K, process time 2 min, and atmosphere — a vacuum.

Both the type of crystal structure and the phase composition of the initial powders and bulk materials were determined by means of x-ray diffraction analysis (XRD, Rigaku Ultima IV diffractometer with $\text{CuK}\alpha$ radiation). Scanning electron microscopy (SEM, Nova NanoSEM 450 microscope) was used to investigate the particle morphology of the original powders and evaluate the average particle size as well as to identify aspects of the grain structure and crystallographic texture of bulk samples. The grain structure of the samples was also studied by means of electron backscatter diffraction (EBSD). The sample surface was prepared by vibration-assisted polishing. A TSL OIM system (Velocity EBSD camera) was used to perform the EBSD analysis; this system was an attachment to a Nova NanoSEM 450 microscope. A Shimadzu ICPE-9000 inductively coupled plasma optical emission spectrometer was used to quantify the Dy content in bulk samples.

EXPERIMENTAL RESULTS

According to the x-ray diffraction data all initial powders with different Dy contents are single-phase and possess a trigonal system characteristic of bismuth telluride (PDF#01-089-2009). All diffraction peaks in the diffraction patterns can be accurately indexed according to space symmetry group $R\bar{3}m$ (166). A typical x-ray diffraction pattern of the initial powder with the composition $\text{Bi}_{1.98}\text{Dy}_{0.02}\text{Te}_{2.7}\text{Se}_{0.3}$ is displayed in Fig. 1a.

For the initial powders the unit cell parameters were determined using the internal standard method (Table 1). It was determined that these parameters naturally decrease with increasing concentration of dysprosium. However, once the maximum concentration of the alloying element is reached, the parameter c is observed to increase, which, in accordance with the published data, can be explained by the partial intercalation of dysprosium into the interpacket space of the structure of compounds based on bismuth telluride [6].

The diffraction patterns of polycrystalline materials obtained from the initial powders corresponded to the diffraction patterns of the initial powders themselves (i.e., the phase

TABLE 1. Concentration C of the Alloying Element Dy, Crystal Lattice Parameters a , c , Average Transverse Size d and Thickness h of Particles of the Original Powders, Average Diameter D and thickness H of the Grains of Bulk Samples

Sample	C (Dy), at.%	$a = b$, Å	c , Å	d , m	h , nm	D , nm	H , nm
$\text{Bi}_2\text{Te}_{2.7}\text{Se}_{0.3}$	0.000	4.382	30.493	666	72	1808	453
$\text{Bi}_{1.999}\text{Dy}_{0.001}\text{Te}_{2.7}\text{Se}_{0.3}$	0.017	4.381	30.485	650	73	1105	282
$\text{Bi}_{1.9975}\text{Dy}_{0.0025}\text{Te}_{2.7}\text{Se}_{0.3}$	0.067	4.379	30.468	617	71	978	256
$\text{Bi}_{1.995}\text{Dy}_{0.005}\text{Te}_{2.7}\text{Se}_{0.3}$	0.160	4.377	30.453	606	70	892	223
$\text{Bi}_{1.99}\text{Dy}_{0.01}\text{Te}_{2.7}\text{Se}_{0.3}$	0.310	4.376	30.433	404	73	830	175
$\text{Bi}_{1.98}\text{Dy}_{0.02}\text{Te}_{2.7}\text{Se}_{0.3}$	0.560	4.375	30.496	378	73	760	169

composition of the initial powders did not change during the sintering process) (Fig. 1b). However, the intensities of various peaks in the diffraction pattern of polycrystalline materials change noticeably. The redistribution of peak intensities is associated with partial ordering of material grains (the development of texturing), which will be discussed below.

It follows from the SEM results that all initial powders consist of particles in the form of hexagonal plates. Figure 2 shows an SEM image of particles of the initial powder with the composition $\text{Bi}_{1.98}\text{Dy}_{0.02}\text{Te}_{2.7}\text{Se}_{0.3}$. To estimate the average transverse size d and the average thickness h of particles in the initial powders, histograms of particle size distribution were constructed and analyzed within the framework of a log-normal unimodal distribution corresponding to the expression [7]

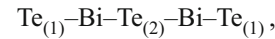
$$F = \frac{1}{\sqrt{2\pi} \ln \sigma} \exp\left(-\frac{\ln d - \ln d_a}{2 \ln^2 \sigma}\right), \quad (1)$$

where F is the log-normal probability density function; $\ln d$ and $\ln \sigma$ are logarithms of the average size and standard deviation of the corresponding sizes. The results of calculations of particle sizes are displayed in Table 1. Since for all values of x the transverse size of the particles is much greater than their thickness, such particles should be considered as two-dimensional (2D) objects.

It is known that the formation of such hexagonal plates of compounds based on Bi_2Te_3 in the process of chemical synthesis from different solutions is associated with the characteristics of the crystal structure and chemical bonds of these compounds [8]. Compounds based on Bi_2Te_3 have a layered crystal structure, and the chemical bonds between atoms within the layers are strong polar covalent bonds and between the layers they are weak van der Waals bonds. As a result, in the process of chemical synthesis the growth rate of particles along the layers turns out to be much greater than the growth rate perpendicular to the layers.

To explain the results of the influence of doping on aspects of the microstructure of $\text{Bi}_{2-x}\text{Dy}_x\text{Te}_{2.7}\text{Se}_{0.3}$ compounds, it is necessary to consider the growth mechanisms of particles of compounds based on bismuth telluride, which are realized during the solvothermal synthesis of the initial powder (for more details, see [9 – 13]). The structure of compounds

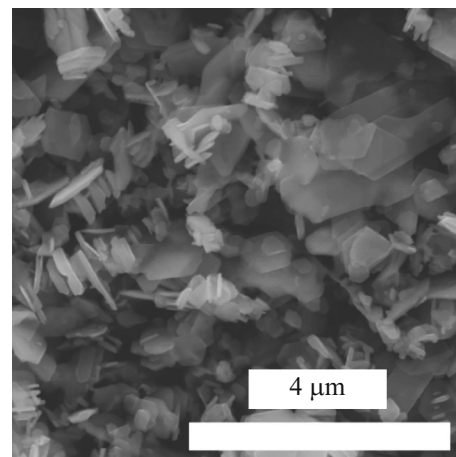
based on Bi_2Te_3 corresponds to the tetradymite type. This structure is usually described in terms of a layered structure where the layers are perpendicular to the c -axis. Five separate atomic layers are packed in the crystal structure in the following order:



where $\text{Te}_{(1)}$ and $\text{Te}_{(2)}$ denote two different positions of tellurium in the lattice.

Bismuth atoms are located at the center of octahedra formed by tellurium atoms, and $\text{Te}_{(2)}$ atoms occupy the center of octahedra formed by bismuth atoms. The $\text{Te}_{(1)}$ atoms are connected, on the one hand, to three Bi atoms by covalent bonds and, on the other hand, by weak van der Waals bonds to three other $\text{Te}_{(1)}$ atoms. The length of the Bi- $\text{Te}_{(1)}$ chemical bond is close to that expected of a covalent bond, while the length of the Bi- $\text{Te}_{(2)}$ bond is more likely to correspond to the value expected for an ionic bond [14, 15].

We can suppose that on the synthesis of $\text{Bi}_{2-x}\text{Dy}_x\text{Te}_{2.7}\text{Se}_{0.3}$ compounds the formation of hexagonal plates will occur during Ostwald ripening. The growth of $\text{Bi}_{2-x}\text{Dy}_x\text{Te}_{2.7}\text{Se}_{0.3}$ particles in the direction perpendicular to the particle plane (along the crystallographic c axis) is controlled by weak van der Waals interaction. Since the particle thickness is practi-

**Fig. 2.** Typical SEM image of the original $\text{Bi}_{1.98}\text{Dy}_{0.02}\text{Te}_{2.7}\text{Se}_{0.3}$ powder.

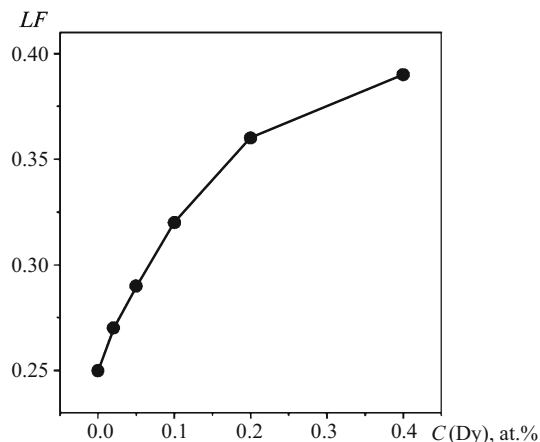


Fig. 3. Lotgering factor versus the concentration of dysprosium for $\text{Bi}_{2-x}\text{Dy}_x\text{Te}_{2.7}\text{Se}_{0.3}$ samples.

cally independent of x (see Table 1), we can conclude that this interaction is insensitive to the dysprosium content in the compounds under study. It is known that the thickness of particles is controlled by the temperature and duration of synthesis [15–17].

A decrease in the average transverse particle size with increasing x could be due to an increase in the polarity of chemical bonds (ionicity of the bond), affecting the process of particle dissolution, which simultaneously operates during the synthesis of particles in polar solvents. Such a mechanism was previously proposed to explain the change in particle size in powders of the Sm-doped compound $\text{Bi}_2\text{Te}_{2.7}\text{Se}_{0.3}$ [18]. The change in the ionicity of the compounds $\text{Bi}_{2-x}\text{Dy}_x\text{Te}_{2.7}\text{Se}_{0.3}$ could be due to the difference in the electronegativities of Bi and Dy (2.02 for Bi and 1.22 for Dy). Using the electronegativity value, the degree of ionicity of a polar covalent bond can be determined using Pauling's formula [8]. For the compounds $\text{Bi}_{2-x}\text{Dy}_x\text{Te}_{2.7}\text{Se}_{0.3}$ the calculated degree of bond ionicity gradually increases from 0.39 for $x = 0.0000$ to 0.44 for $x = 0.0200$. The size of particles during the growth process is determined by the competition of two simultaneously acting but oppositely directed processes — the chemical synthesis of particles effecting an increase in size and their dissolution effecting size reduction is determined by the condition of dynamic equilibrium of these processes. The dissolution process is based on electrostatic interaction between ions in growing particles and polar solvent molecules [18]. An increase in the proportion of bond ionicity effects a stronger interaction and a corresponding increase in the efficiency of the dissolution process. As a result, the average particle diameter will decrease with increasing Dy content.

An elemental analysis of samples with different Dy contents, also given in Table 1, allows us to conclude that the actual composition of all samples is close to the nominal composition.

The density of bulk samples, determined using the Archimedes method, was practically independent of the doping level and was equal to 7.5 g/cm^3 , which is about 96% of the theoretical density (7.78 g/cm^3) [8].

It was found that all bulk polycrystalline samples are textured during the sintering process. Texturing is easily observed in diffraction patterns of samples obtained from surfaces that are oriented perpendicular ('perpendicular' surface) or parallel ('parallel' surface) to the direction of application of pressure during the sintering process. This direction is the texture axis. Although all the peaks in the diffraction patterns correspond to the structure $R\bar{3}m$, i.e., the positions of the peaks do not depend on the direction of application of pressure, their intensities in the diffraction patterns taken from the perpendicular and parallel surfaces are noticeably redistributed. An increase in the intensity of the $(00l)$ peaks is observed on the 'perpendicular' surface (Fig. 1b). This redistribution of peak intensities could be associated with the formation of a lamellar structure with a predominant orientation of grains in a plane parallel to the pressing direction. The degree of preferred grain orientation (degree of texturing) for textured samples can be assessed using the Lotgering factor LF [8]. The LF value for bulk samples with different dysprosium contents was estimated by analyzing the x-ray diffraction patterns using the expressions

$$LF = \frac{p - p_0}{1 - p_0}, \quad (2a)$$

where p and p_0 are defined as

$$p = \frac{I(00l)}{\sum I(hkl)} \quad \text{or} \quad p_0 = \frac{I_0(00l)}{\sum I_0(hkl)}, \quad (2b)$$

where intensities I and I_0 correspond to textured and non-textured samples, respectively. In the limit $LF \rightarrow 1$ for samples with an ideal texture (for example, single crystals) and $LF \rightarrow 0$ for completely non-textured samples (powder or polycrystalline material with completely random grain orientation).

It can be seen that an increase in the concentration of dysprosium effects gradual reduction in the Lotgering factor from about 0.25 for $x = 0.00$ to about 0.38 for $x = 0.02$ (Fig. 3).

It was also found that the average grain size in textured samples of $\text{Bi}_{2-x}\text{Dy}_x\text{Te}_{2.7}\text{Se}_{0.3}$ strongly depends on the Dy content. To determine the average grain size, SEM images of sample surfaces oriented perpendicular or parallel to the direction of application of pressure during the sintering process were analyzed.

Figure 4 shows such images of perpendicular and parallel surfaces for the non-doped compound $\text{Bi}_2\text{Te}_{2.7}\text{Se}_{0.3}$ (Fig. 4a and b) and the compound $\text{Bi}_{1.98}\text{Dy}_{0.02}\text{Te}_{2.7}\text{Se}_{0.3}$ with the maximum doping level (Fig. 4c and d). Perpendicular surfaces (Figs. 4a and c) are characterized by a disordered

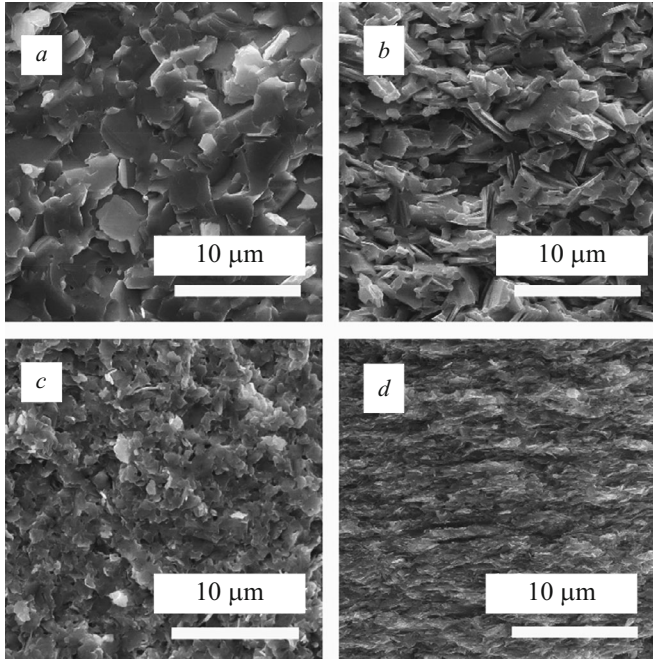


Fig. 4. SEM images obtained from the cleavage surfaces of $\text{Bi}_2\text{Te}_{2.7}\text{Se}_{0.3}$ (top image) and $\text{Bi}_{1.98}\text{Dy}_{0.02}\text{Te}_{2.7}\text{Se}_{0.3}$ (bottom image) samples oriented perpendicular (*a* and *c*) and parallel (*b* and *d*) to the direction of pressure application for the non-alloyed compound Bi_2Te .

grain structure, represented by grains of predominantly irregular shape. For a parallel surface the grains form an ordered lamellar structure, the lamellar sheets lying in a plane perpendicular to the pressing direction (Fig. 4*b* and *d*). This grain ordering reduces the deformation created by uniaxial compression during spark plasma sintering. Thus, the SEM results (see Fig. 4) are in good agreement with the XPA re-

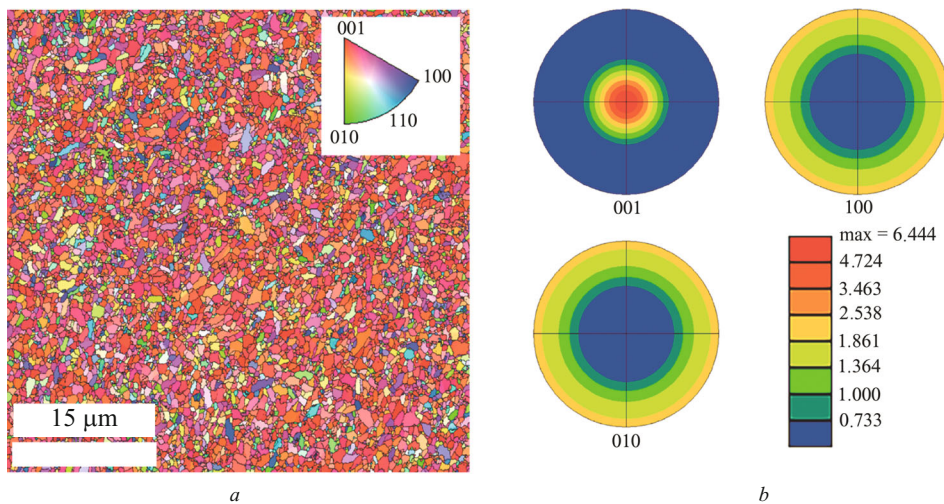


Fig. 5. Maps of the distribution of grain orientations (*a*) and pole figures (*b*) for the sample $\text{Bi}_{1.98}\text{Dy}_{0.02}\text{Te}_{2.7}\text{Se}_{0.3}$ as obtained from a surface oriented perpendicular to the direction of application of pressure during the sintering process. Inset: a stereographic triangle with color indication of crystallographic directions.

sults (see Fig. 1). Comparing the SM images for the compounds $\text{Bi}_2\text{Te}_{2.7}\text{Se}_{0.3}$ and $\text{Bi}_{1.98}\text{Dy}_{0.02}\text{Te}_{2.7}\text{Se}_{0.3}$, we can conclude that doping leads to a significant reduction in grain size. For textured samples the grain sizes in the directions perpendicular (transverse grain size D) and parallel (grain thickness H) to the direction of application of pressure (either along or across the lamellar sheets) differ significantly, i.e., the grains are elongated along the sheets. To determine the average grain size D and H , corresponding histograms of the distribution of grains by these sizes were constructed, which were analyzed within the framework of the lognormal unimodal distribution (expression (1)). The values of D and H for samples with different Dy contents are given in Table 1. It is clear that as x increases, the grain size decreases.

It is helpful to compare the effect of Dy alloying on the average particle size in the initial powders of the compounds $\text{Bi}_{2-x}\text{Dy}_x\text{Te}_{2.7}\text{Se}_{0.3}$ and the average grain size in the corresponding textured samples obtained from these powders. First of all, there is a clear correlation between these sizes: a decrease in particle size on alloying effects a corresponding reduction in grain size. Secondly, as for particles, the transverse size of the grain turns out to be much larger than their thickness, i.e., like particles, grains are 2D objects. Thirdly, the average grain size is much larger than the average particle size, which is associated with recrystallization processes during high-temperature sintering of polycrystalline materials. Thus, it can be concluded that the average size and shape of grains in textured compounds $\text{Bi}_{2-x}\text{Dy}_x\text{Te}_{2.7}\text{Se}_{0.3}$ compounds with different Dy contents are determined by the average size and shape of particles in the corresponding initial powders used for spark plasma sintering.

The average grain size can be determined and the formation of crystallographic texture in the compounds $\text{Bi}_{1.98}\text{Dy}_{0.02}\text{Te}_{2.7}\text{Se}_{0.3}$ can be confirmed by using the EBSD method. This method was used to study the surface of samples oriented perpendicular to the direction of application of pressure during the sintering process. As an example, Fig. 5 shows maps of the distribution of crystallographic orientations of grains (Fig. 5*a*) and pole figures (Fig. 5*b*) for the $\text{Bi}_{1.98}\text{Dy}_{0.02}\text{Te}_{2.7}\text{Se}_{0.3}$ sample. For all samples with different Dy contents, the grain size D calculated based on the distribution maps of grain orientations corresponds to the results obtained from the analysis of SEM images. Figure 5*b* shows pole figures of three representative crystallographic directions. High pole density is associated with texture formation. Simi-

lar grain ordering can also be seen in the (100) and (010) pole figures.

The relationship ascertained in this work between particles in the original powders and grains in textured samples of the compound $\text{Bi}_{2-x}\text{Dy}_x\text{Te}_{2.7}\text{Se}_{0.3}$ with different Dy contents was previously discovered and analyzed for the compound doped with Sm [18]. In particular, in [18] it was found that the degree of texturing of samples increased with increasing Sm content. A similar effect was found for the compounds $\text{Bi}_{2-x}\text{Dy}_x\text{Te}_{2.7}\text{Se}_{0.3}$ compounds (see Fig. 3).

Following [18], this effect, which takes into account the change in grain size during alloying (see Table 1), can be explained as follows. The initial process of spark plasma sintering of initial powders is a particle packing process, which includes a rotation stage (particles in the form of one-dimensional plates with the initial powder under the influence of uniaxial pressure rotate through a certain angle, trying to line up parallel to one another), and a sliding stage (contacting particles in the process of parallel alignment slide along the plane of contact). The ideal texture in bulk polycrystalline samples will be achieved when the particles in the original powder are aligned strictly parallel during the packaging process. Particle size reduction means that the sliding step will result in greater particle ordering (and a subsequent increase in texturing) on account of the reduction in sliding path.

CONCLUSIONS

An increase in the Dy content in the polycrystalline compound $\text{Bi}_{2-x}\text{Dy}_x\text{Te}_{2.7}\text{Se}_{0.3}$ with $x = 0.0000, 0.0010, 0.0025, 0.0050, 0.0100,$ and 0.0200 is accompanied by the following changes in the microstructure (grain structure):

- 1) reduction in the average grain size;
- 2) increase in the degree of texturing.

These changes in the grain structure can affect the thermoelectric properties of the compound. The change in the average grain size is determined by the corresponding changes in the average particle size in the original powders, which in turn is associated with a change in the degree of ionicity of the chemical bond during alloying. An increase in the degree of texturing is associated with a decrease in the average grain size in the samples, which contributes to more efficient packing of particles of the original powders under the influence of uniaxial pressure in the process of spark plasma sintering.

This work was carried out with the financial support of the Russian Science Foundation under grant No. 21-73-00199. The equipment of the Center for Collective Use of Scientific Equipment "Technologies and Materials" of the National Research University "BelSU" and the equipment of the Center for High Technologies of the V. G. Shukhov Belarusian State Technical University was used.

REFERENCES

1. L. E. Bell, "Cooling, heating, generating power, and recovering waste heat with thermoelectric systems," *Science*, **321**(5895), 1457 – 1461 (2008).
2. M. Yaprntsev, A. Vasil'ev, and O. Ivanov, "Thermoelectric properties of the textured $\text{Bi}_{1.9}\text{Gd}_{0.1}\text{Te}_3$ compounds spark-plasma-sintered at various temperatures," *J. Eurp. Ceram. Soc.*, **40**(3), 742 – 750 (2020).
3. M. C. Hsiao, Sh.-H. Liao, M.-Yu Yen, et al., "Preparation of covalently functionalized graphene using residual oxygen-containing functional groups," *ACS Appl. Mater. Interf.*, **2**(11), 3092 – 3099 (2010).
4. O. Ivanov and M. Yaprntsev, "Mechanisms of thermoelectric efficiency enhancement in Lu-doped Bi_2Te_3 ," *Mater. Res. Express*, **5**(1), 015905 (2018).
5. Z. Li, Ch. Xiao, H. Zhu, and Yi. Xie, "Defect chemistry for thermoelectric materials," *J. Am. Chem. Soc.*, **138**(45), 14810 – 14819 (2016).
6. T. Kristiantoro, D. Mada, and V. Fauzia, "The influence of Dy concentration on the thermoelectric properties of *n*-type Dy-doped Bi_2Te_3 pellets prepared by hydrothermal and carbon burial sintering," *J. Phys. Chem. Solids*, **158**, 110241 (2021).
7. O. D. Neikov, D. V. Lotsko, and V. G. Gopienko, "Powder characterization and testing," in: *Handbook of NonFerrous Metal Powders: Technologies and Applications*, Elsevier, Oxford (2009).
8. A. Vasil'ev, O. Ivanov, E. Danshina, and M. Yaprntsev, "Anisotropic thermoelectric properties of $\text{Bi}_{1.9}\text{Lu}_{0.1}\text{Te}_{2.7}\text{Se}_{0.3}$ textured via spark plasma sintering," *Solid State Sci.*, **84**, 28 – 43 (2018).
9. T. Ludwig, L. Guo, P. McCrary, et al., "Mechanism of bismuth telluride exfoliation in an ionic liquid solvent," *Langmuir*, **31**(12), 3644 – 3652 (2015).
10. B. Hamawandi and M. Kuchowicz, "Facile solution synthesis, processing and characterization of *n*- and *p*-type binary and ternary Bi-Sb tellurides," *Appl. Sci.*, **10**(3), 1178 (2020).
11. D.-D. Li, X.-Y. Qin, Y.-F. Liu, et al., "Improved thermoelectric properties for solution grown $\text{Bi}_2\text{Te}_{3-x}\text{Se}_x$ nanoplatelet composites," *RSC Adv.*, **3**(8), 2632 – 2638 (2013).
12. M. Loor, G. Bendt, U. Hagemann, et al., "Synthesis of Bi_2Te_3 and $(\text{Bi}_x\text{Sb}_{1-x})_2\text{Te}_3$ nanoparticles using the novel IL $[\text{C}_4\text{mim}]_3[\text{Bi}_3\text{I}_{12}]$," *Dalton Trans.*, **45**(39), 15326 – 15335 (2016).
13. X. B. Zhao, X. H. Ji, Y. H. Zhang, et al., "Hydrothermal synthesis and microstructure investigation of nanostructured bismuth telluride powder," *Appl. Phys. A*, **80**, 1567 – 1571 (2005).
14. J. R. Drabble and C. H. L. Goodman, "Chemical bonding in bismuth telluride," *J. Phys. Chem. Solids*, **5**(1–2), 142 – 144 (1958).
15. S. Nakajima, "The crystal structure of $\text{Bi}_2\text{Te}_{3-x}\text{Se}_x$," *J. Phys. Chem. Solids*, **24**(3), 479 – 485 (1963).
16. Z. Wu, M. Erzhen, Z. Wan, et al., " Bi_2Te_3 nanoplates' selective growth morphology on different interfaces for enhancing thermoelectric properties," *Crys. Growth Design*, **19**(7), 3639 – 3646 (2019).
17. Z. Wang, X. Zhang, Z. Zeng, et al. "Two-step molecular beam epitaxy growth of bismuth telluride nanoplate thin film with enhanced thermoelectric properties," *ECS Solid State Lett.*, **3**(8), 99 (2014).
18. M. Yaprntsev, O. Ivanov, A. Vasil'ev, et al., "Effect of Sm-doping on microstructure and thermoelectric properties of textured *n*-type $\text{Bi}_2\text{Te}_{2.7}\text{Se}_{0.3}$ compound due to change in ionic bonding fraction," *J. Solid State Chem.*, **297**, 122047 (2021).